© 2019. Published by The Company of Biologists Ltd | Journal of Experimental Biology (2019) 222, jeb203125. doi:10.1242/jeb.203125

RESEARCH ARTICLE

Selection for longer limbs in mice increases bone stiffness and brittleness, but does not alter bending strength

Miranda N. Cosman[1], Hayley M. Britz[2,3] and Campbell Rolian[3,4,*]

ABSTRACT

The ability of a bone to withstand loads depends on its structural and material properties. These tend to differ among species with different modes of locomotion, reflecting their unique loading patterns. The evolution of derived limb morphologies, such as the long limbs associated with jumping, may compromise overall bone strength. We evaluated bone mechanical properties in the Longshanks mouse, which was selectively bred for increased tibia length relative to body mass. We combined analyses of 3D shape and cross-sectional geometry of the tibia, with mechanical testing and bone composition assays, to compare bone strength, elastic properties and mineral composition in Longshanks mice and randomly bred controls. Our data show that, despite being more slender, cortical geometry and predicted bending strength of the Longshanks tibia were similar to controls. In whole bone bending tests, measures of bone bending strength were similar across groups; however, Longshanks tibiae were significantly more rigid, more brittle, and required less than half the energy to fracture. Tissue-level elastic properties were also altered in Longshanks mice, but the bones did not differ from the control in water content, ash content or density. These results indicate that while Longshanks bones are as strong as control tibiae, selection for increased tibia length has altered its elastic properties, possibly through changes in organic bony matrix composition. We conclude that selection for certain limb morphologies, and/or selection for rapid skeletal growth, can lead to tissue-level changes that can increase the risk of skeletal fracture, which in turn may favor the correlated evolution of compensatory mechanisms to mitigate increased fracture risk, such as delayed skeletal maturity.

KEY WORDS: Artificial selection, Bone cross-sectional geometry, Bone stiffness, Bone strength, Longshanks mouse

INTRODUCTION

Bone fractures are an important disease burden in humans and domesticated animals (Gregory and Wilkins, 1989; Fleming et al., 1994; Bouxsein, 2005; Ramzan and Palmer, 2011), and the ability to withstand bone fractures throughout life likely also impacts the evolutionary fitness of wild animals (Bramblett, 1967; Taylor, 1971; Lovell, 1991; Jurmain, 1997; ter Hofstede et al., 2003; Forsman et al., 2006; Carter et al., 2008). The ability of a bone to withstand external loading depends on its material properties, size and shape, especially its cross-sectional geometry (Rubin, 1984; Jepsen et al., 2003; O'Neill and Ruff, 2004; Felsenberg and Boonen, 2005; Hernandez and Keaveny, 2006). Long bone cross-sectional geometries often differ between species that use different locomotor repertoires. This variation in bone structure may reflect differences in where and how loads are distributed across a bone (Bou et al., 1987; Bou et al., 1991; Cubo and Casinos, 1998; Christiansen, 1999a,b; Young et al., 2014), though this relationship does not always hold (Biewener and Bertram, 1994; Demes et al., 1998; Demes et al., 2001; Lieberman et al., 2004; Wallace et al., 2014). Cross-sectional geometry and other bone properties (e.g. trabecular orientation) can also change over a lifetime in response to specific loading patterns (Biewener and Bertram, 1994; Heinrich et al., 1999; Lieberman et al., 2003; Ruff, 2003; Pontzer et al., 2006; Main and Biewener, 2007; Young et al., 2010; Ruff et al., 2013; Sarringhaus et al., 2016). At the same time, however, the adaptive evolution of limb bone morphologies in specific locomotor contexts may also be constrained by other organismal traits such as body mass or skeletal size, leading to potential trade-offs in the strength of individual limb bones.

The Longshanks mouse was selectively bred for longer tibiae relative to body mass. In 20 generations, we produced two independent lines of Longshanks mice (hereafter LS1 and LS2) in which the tibia is ∼13–15% longer than randomly bred control mice from the same genetic background (CD-1, hereafter control mice), but body masses remain unchanged (Marchini et al., 2014). In our previous study using only LS1, we demonstrated that tibia length increased without a commensurate change in its cross-sectional geometry (i.e. with negative allometry) (Cosman et al., 2016). Specifically, the tibia's cross-sectional area and polar section modulus in LS1 did not change appreciably, which led us to predict that it is significantly less resistant to bending moments. In a related study (Farooq et al. 2017), we found that tibia trabecular microarchitecture had been substantially altered in parallel with increases in tibia length in both Longshanks lines, potentially altering its ability to withstand compressive loads. In the present study, we investigated whether the altered shape of the Longshanks tibia has impacted its strength and elastic properties. We performed three complementary analyses. First, we evaluated 3D shape of the tibia as well as its cross-sectional properties at the midshaft in the three lines. This analysis extends our previous study (Cosman et al., 2016) by including both Longshanks replicates, and by examining whether shape changes persisted in Longshanks at F15, i.e. after an additional five generations of selective breeding. We tested the hypothesis that bone shape and cross-sectional properties (e.g. cross-sectional area) did not differ significantly among the three lines (Cosman et al., 2016). Second, we assessed the mechanical strength and elastic properties of the bones using a three-point bending test to test the hypothesis that there are no differences in these traits among

[1]Department of Anthropology, University of Michigan, 101 West Hall 1085 S. University Ave, Ann Arbor, MI 48109, United States. [2]Department of Cell Biology and Anatomy, Cumming School or Medicine, University of Calgary, 3330 Hospital Drive NW, Calgary, Alberta, T2N 4N1, Canada. [3]McCaig Institute for Bone and Joint Health, University of Calgary, 3330 Hospital Drive NW, Calgary, Alberta, T2N 4N1, Canada. [4]Department of Comparative Biology and Experimental Medicine, Faculty of Veterinary Medicine, University of Calgary, 3330 Hospital Drive NW, Calgary, Alberta, T2N 4N1, Canada.

*Author for correspondence (cprolian@ucalgary.ca)

C.R., 0000-0002-7242-342X

Received 7 March 2019; Accepted 24 April 2019

the three lines. Finally, we compared tissue-level bone composition among the lines in terms of water and mineral content.

MATERIALS AND METHODS

Samples

All animal procedures were approved by the Health Sciences Animal Care Committee at the University of Calgary (protocol AC13-0077). Mice from the F15 and F16 generations of the Longshanks experiment were used in this study. Details of the selection experiment are provided elsewhere (Marchini et al., 2014). All Longshanks and control mice are derived from CD-1 outbred stock. At both generations, Longshanks tibiae were ∼12–14% longer than those in controls, but there were no differences in mean body mass among lines. For assessing whole bone and tissue-level mechanical properties, we collected sex-balanced samples of mice that were not selected as breeders for the following generation (sample sizes: LS1, n=42; LS2, n=38; control, n=36). To examine bone tissue composition, we sampled non-breeder females from generation F16 (n=8 per line).

Micro-computed tomography (μCT) scans

Following euthanasia at 56–63 days (by CO_2 inhalation), mice were weighed to the nearest 0.01 g and packed into Styrofoam tubes, and whole body μCT scans were acquired on a Skyscan 1173 μCT scanner (Bruker, Kontich, Belgium) at an isotropic resolution of 45 μm (70 kV voltage and 114 μA current). 3D image stacks were reconstructed in NREcon v1.6.9 (Bruker, Kontich, Belgium) for shape and cross-sectional analyses.

3D shape analysis

Image stacks were imported into Amira v5.4.2 (Visage Imaging, Berlin, Germany) and an Amira mesh file (.am) of the hind limb was created for shape analysis. A set of 12 3D landmarks were placed on homologous anatomical structures at the proximal and distal epiphyses, as well as the tibia–fibula junction, in the scans of the right tibia from each mouse. The protocol for shape, including reliability and measurement error of landmark placements, and geometric morphometric analysis, are described in Cosman et al. (2016). The distance between the landmarks at the cranial point of the proximal epiphysis and on the caudal medial tip of the medial malleolus was used as a measure of tibia length.

Cross-sectional area and properties

The Amira mesh file was imported into ImageJ 1.51p (National Institutes of Health, Bethesda, Maryland) (Rasband, 2014). To account for different whole body scan positions, the stacks were first aligned vertically (parallel to long axis of tibia), using the Interactive Stack Rotation plugin in ImageJ. Following an automatic thresholding procedure, we used the BoneJ plugin (Doube et al., 2010) to obtain cross-sectional properties from a slice at the distal tip of the tibial tuberosity, i.e. the same approximate area that underwent mechanical testing. Following the recommendations in Jepsen et al. (2015), we obtained periosteal area (total area, Tt.Ar., in mm^2), cortical area (Ct.Ar., in mm^2), bone marrow area (i.e. endosteal area, Ma.Ar, in mm^2), relative cortical area (Ct.Ar/Tr.Ar), mean cortical thickness (Ct.Th), the minimum and maximum moments of inertia (I_{min} and I_{max}, respectively, in mm^4) and the polar section modulus (Z_P, in mm^3) at the selected slice. As in our previous study (Cosman et al., 2016), we calculated an index of robusticity (IR) by taking the ratio of Z_P (in mm^3) to the product of bone length (in mm) and body mass (in $mg^{2/3}$) (Polk et al., 2000; Ruff, 2000; Young et al., 2014) to evaluate the tibia's bending strength in relation to its length and the mass of the animal.

Whole bone mechanical properties

A sex-balanced subsample of 82 mice was used for mechanical testing (sample sizes by sex: LS1, 15F/13M; LS2, 15F/15M; Control, 12F/14M). Mechanical testing was performed on the same day an individual mouse was scanned. After scanning, the left hind limb was skinned and removed, and dissected free of soft tissue. The bones were then subjected to a three-point bend test on an ElectroForce 3230 testing machine (Bose Corp., Eden Prairie, USA). The end fixtures (supporting points) were placed 6 mm apart in LS1 and LS2 and 4 mm apart in the control line. This difference of 2 mm, which is approximately equal to the mean length difference between Longshanks and control tibiae (see Results), ensured that bones were loaded at anatomically homologous locations in the three lines.

The center support (crosshead) was placed on the lateral side at the level of the distal end of the tibial tuberosity, corresponding to where cross-sectional properties were measured. The left support was on the tibial metaphysis and the right was placed immediately proximal to the tibia–fibula junction. The bottom fixtures were attached to a 450 N load cell, and the crosshead moved at a constant displacement rate of 2 mm min^{-1}. The tibiae were bent medio-laterally in the transverse plane as this orientation improved stability of the bone on the test fixtures. To minimize bone movement prior to the bending test, a preload of 1 N was applied, which did not cause any visible deformation of the bone. The bones were then loaded until they fractured.

Whole bone bending tests

Moment-normalized displacement curves

All mechanical testing analyses were conducted using custom-written scripts in MATLAB (R2017b, Natick, MA). Three-point bending tests generate load–displacement curves that record how much force a structure can withstand before fracturing, under continuous displacement of the tester's crosshead. Because our fixture span lengths were not the same size in Longshanks and control mice, however, their load-displacement curves are not directly comparable. Normalizing both load and displacement for fixture geometry is required for two reasons. First, mechanical testers measure loads experienced by the bone, but whole-bone strength is ultimately determined by bending moments, which are a function of the distance between the tester's supports (i.e. load arms) (Jepsen et al., 2015). Second, for a given displacement of the crosshead, a bone bent on a shorter span deflects substantially more than a bone bent on a longer span. Accordingly, identical recorded displacements to fracture in these two bones would lead one to conclude erroneously that the bones are equally ductile, when in fact the bone on the shorter span undergoes more deformation before failing. Hence, we converted the bending data to moment-normalized displacement curves following Jepsen et al. (2015). Moments of force were obtained using the following equation:

$$\mathbf{M} = \frac{\mathbf{F} \times L}{4}, \quad (1)$$

where $\mathbf{M}$ is the moment of force, in N mm, $\mathbf{F}$ is the force, and L is the span length between the two bottom points of the testing apparatus (6 mm for Longshanks, 4 mm for controls). The displacement d was normalized as follows, and is expressed in units of mm mm^{-2}:

$$d' = \frac{12d}{L^2}. \quad (2)$$

Moment-normalized displacement curves ($\mathbf{M}$–d') were used to obtain yield moment, at which deformation becomes plastic

(see below), as well as the maximum moment and moment at fracture.

Rigidity, post-yield displacement and work-to-fracture

Rigidity of the tibia, in N mm^{-2}, describes the amount of elastic deformation the bone undergoes as a function of the moments applied. Rigidity is derived from moment-normalized displacement and is the fixture-normalized equivalent of whole bone stiffness derived from load–displacement plots (Jepsen et al., 2015). Rigidity was obtained as the slope of a linear regression fitted to the initial linear portion of the $\mathbf{M}$–d' curves. The linear regression was fit to the points between 15 and 25% of fracture displacement, as $\mathbf{M}$–d' curves for some individuals departed from linearity after ∼30% displacement. Yield was defined as the point at which a regression line representing a 10% loss in rigidity intersects the $\mathbf{M}$–d' curve. Normalized post-yield displacement (PYD), in mm mm^{-2}, was defined as the normalized displacement between yield and fracture. Finally, work-to-fracture, in N, which reflects the overall bending resistance of a structure, was obtained by integrating the area under the total $\mathbf{M}$–d' curves (Jepsen et al., 2015).

Bone tissue mechanical properties

Mechanical properties of bone tissue can be estimated from bending tests, using expectations derived from engineering beam theory (Turner and Burr, 1993; Jepsen et al., 2015). These estimates must be interpreted with caution, however, because bones are not perfect cylinders of equal thickness throughout the cortex, and their bending behavior can depart significantly from beam theory predictions (van Lenthe et al., 2008). Still, tissue-level estimates obtained from three-point bending tests can provide a 'first-pass' approximation of differences among groups when homologous bones are compared under similar testing conditions. We used the force–displacement relationships to obtain stress (σ), strain (ε) and the elastic modulus (E) using the following equations:

$$\sigma = \frac{\mathbf{F} \times L \times c}{4I}, \tag{3}$$

$$\varepsilon = \frac{12c \times d}{L^2}, \tag{4}$$

$$E = \frac{K \times L^3}{48I}, \tag{5}$$

where σ is stress, in N mm^{-2} (MPa), ε is strain (unitless), E is elastic modulus (MPa), L is span length (mm), d is raw displacement of the testing apparatus (mm), c (mm) is the distance from the bone cross-section's centroid to the outermost point on the cortex, I is the moment of inertia of the cross-section around the bending axis, and K is stiffness (N mm^{-1}), i.e. the slope of the linear portion of the raw force-displacement plots, derived using the same method as above for rigidity. Because tibiae were bent in a medio-lateral plane, we took c to be half the minimum caliper diameter and I to be I_{max}, both obtained from BoneJ's cross-sectional geometry output (see above). We used the stress–strain curves to derive yield strength and ultimate strength using the same method as above for yield and maximum moments.

Bone tissue composition

The left tibiae of previously frozen F16 female mice were dissected and cleared of soft tissue (n=8 per line, each comprising four pairs of siblings from separate families). Bones were trimmed to obtain sections of tibia diaphysis, by sectioning the bones with a razor blade distal to the proximal metaphysis, and immediately proximal to the tibia–fibula junction. The tibia sections were flushed with water to expel marrow. To obtain hydrated tissue mass, the bones were centrifuged at 5000 ***g*** for 5 min, and weighed to the nearest 0.1 mg on an analytical balance. Dry tissue mass was determined after drying the bone sections overnight at 60°C. Next, the bone segments were scanned on a Skyscan 1173 µCT scanner (Bruker, Kontich, Belgium) at an isotropic resolution of 10 µm (70 kV voltage and 114 µA current). 3D image stacks were reconstructed in NREcon v1.6.9 (Bruker, Kontich, Belgium), and the 'Volume Fraction' module in BoneJ was used to obtain dry bone volume. Finally, ash mass was obtained after ashing the bones in a muffle furnace at 600°C for 24 h. Dry bone density was obtained as dry bone mass (mg) divided by dry bone volume (mm^3). Water and ash content measures were expressed as a percentage of hydrated mass assuming a water density of 1 (Jepsen et al., 2001). Raw data for all shape, cross-sectional, strength and ash analyses can be found in Dataset 1.

Statistical analysis

Tibia shape

Geometric morphometric analyses were carried out in MorphoJ v104a (Klingenberg, 2011). The 12-variable 3D landmark dataset was first subjected to a general least-squares Procrustes superimposition (Dryden and Mardia, 1998; Slice, 2005). Shape differences between the groups were explored by means of principal components analysis (PCA) on Procrustes shape variables. Statistical significance of any difference in mean shape was assessed by pairwise discriminant function analyses (DFA), followed by permutation tests (1000×), as implemented in MorphoJ. Changes along principal components were visualized by means of deformations of wireframes that described shape in the medio-lateral, antero-posterior and proximo-distal epiphyseal profiles of the tibia.

Cross-sectional, whole bone and tissue properties

All statistical analyses were performed in MATLAB using custom scripts (R2017b, Natick, MA). Cross-sectional and strength properties were compared among the three groups using analyses of covariance (ANCOVA), with mouse line and sex as categorical factors, and body mass as a covariate representing an animal's overall size. Our preliminary analyses showed that, aside from bending moments (see Results), there was no interaction between sex and line for bone geometric and strength properties, thus all subsequent statistical analyses were carried out on samples with sexes pooled within lines. We used Tukey's *post hoc* tests to test for statistical significance of pairwise differences in the marginal means among the lines. Differences among females in the F16 lines in tissue density and composition were determined using ANOVAs, followed by Tukey's *post hoc* tests. In all tests, an alpha value of less than 0.05 was considered statistically significant.

RESULTS

Morphometrics and 3D shape

The sample of LS1 mice used in this study was significantly heavier than the other lines (Table 1), even though mean body mass among the complete F15 populations was the same (data not shown). This discrepancy is most likely a stochastic artifact of subsampling from the lines. Among lines (pooled by sex), mean tibia length was ∼13% greater in Longshanks, but did not differ between LS1 and

Journal of Experimental Biology (2019) 222, jeb203125. doi:10.1242/jeb.203125

Table 1. Least squares means and standard errors of the cross-sectional properties at the tibia midshaft in the three lines, estimated at the covariate mean (body mass, 36.32 g)

Property	LS1 (n=42)	LS2 (n=37)	Control (n=36)
Body mass (g)	38.03 (0.78)^{LS2,C}	35.65 (0.54)^{LS1}	34.92 (0.75)^{LS1}
Tibia length (mm)	20.13 (0.09)^{C}	20 (0.09)^{C}	17.86 (0.09)^{LS1,LS2}
Ct.Ar. (mm^2)	1.37 (0.03)	1.41 (0.03)	1.41 (0.03)
Ma.Ar. (mm^2)	0.71 (0.03)^{LS2,C}	0.82 (0.03)^{LS1,C}	0.61 (0.03)^{LS1,LS2}
Tt.Ar. (mm^2)	2.08 (0.05)	2.23 (0.05)^{C}	2.02 (0.05)^{LS2}
Rel. cortical area (Ct.Ar/Tt.Ar.)	0.66 (0.01)^{LS2,C}	0.63 (0.01)^{LS1,C}	0.7 (0.01)^{LS1,LS2}
Ct.Th. (mm)	0.35 (0.01)	0.35 (0.01)	0.37 (0.01)
Min. caliper diameter (mm)	1.47 (0.02)	1.52 (0.02)	1.47 (0.02)
Max. caliper diameter (mm)	2.52 (0.03)	2.52 (0.03)	2.48 (0.03)
I_{min} (mm^4)	0.21 (0.01)	0.24 (0.01)	0.21 (0.01)
I_{max} (mm^4)	0.62 (0.02)	0.66 (0.03)	0.59 (0.03)
Z_P (mm^3)	0.59 (0.02)	0.64 (0.02)^{C}	0.57 (0.02)^{LS2}
Robusticity*	0.27 (0.01)	0.29 (0.01)	0.29 (0.01)

Superscripts denote significant differences in LS means (P<0.05) between a given group and: ^{C}Control, ^{LS1}Longshanks 1, ^{LS2}Longshanks 2 (Tukey's HSD).
*Values for robusticity have been multiplied by 10^5 to improve readability.

LS2. In terms of 3D shape, both Longshanks lines were significantly different from control in mean shape [DFA, mean Procrustes distances: 0.024 (LS1 versus C), 0.019 (LS2 versus C), both permutation test T-square statistics, P<0.001]. As in our previous analysis conducted on F10 tibiae (Cosman et al., 2016), F15 LS1 tibiae were more gracile, with relatively smaller cross-sectional area of the proximal epiphysis, and narrower proximal shafts in the craniocaudal direction (Fig. 1). Our analysis also showed a similar gracilization in LS2 tibiae. Interestingly, however, DFA also showed that LS1 and LS2 differed in mean shape (mean Procrustes distance: 0.012, T-square statistic: 171.5, P=0.003), with LS1 having slightly more gracile cross-sections (Fig. 1).

Cross-sectional geometry

Cross-sectional properties of the tibia mid-shaft in all three lines (sexes pooled) are broadly similar. One notable difference is the endosteal area (Ma.Ar.), which was significantly greater in the Longshanks lines compared with the control (Table 1). Coupled with marginally larger periosteal areas, these larger endosteal areas contribute to significantly lower relative cortical areas in Longshanks (Ct.Ar./Tt.Ar.). The minimum and maximum moments of inertia were not significantly different among lines, nor was the mean index of robusticity, suggesting that the whole bone bending strength based on geometric properties, length of the tibia and body mass should be similar among the lines.

Whole bone material properties in bending

In the bending tests, the tibiae of several individuals did not fracture before the bottom and top supports came into contact. In this situation, displacement becomes limited but the moments continue to be experienced by the bone at a constant rate, leading to incorrect estimates for the post-yield displacements and work-to-fracture. Consequently, we removed these individuals from all strength analyses (n=17). Within line, twice as many control individuals were removed from the analysis (LS1: 4/27, LS2: 4/29, C: 9/26; 3-group chi-square test, χ^2=4.47, P=0.107).

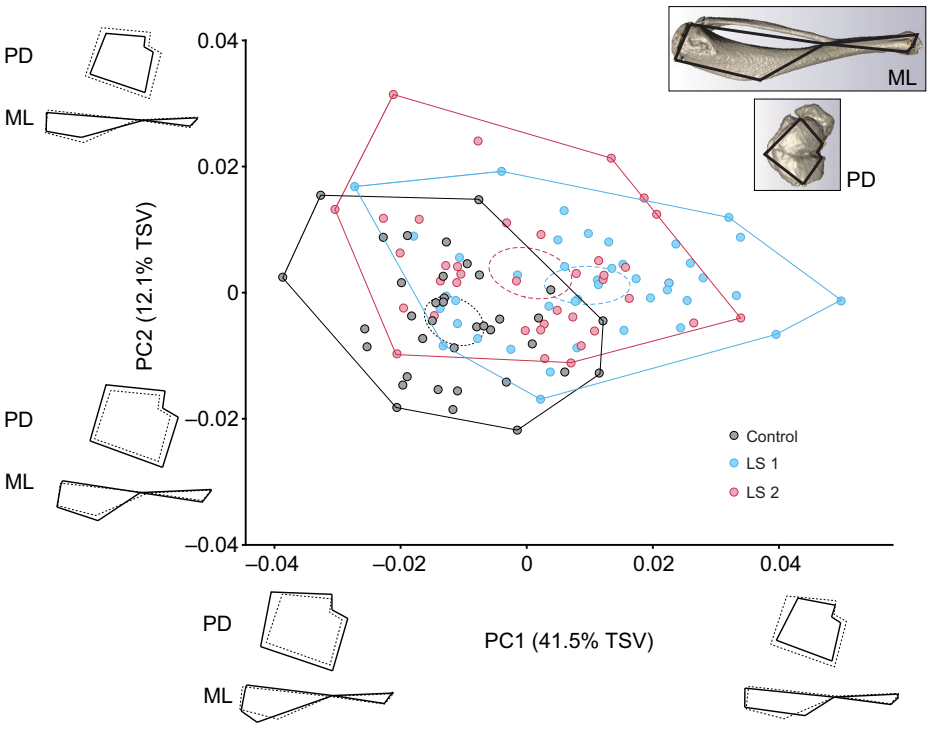

Fig. 1. Scatterplots of the first two principal components (PCs) of the Procrustes shape coordinates of the tibia. Ellipses represent the 95% confidence intervals of the mean PC scores of each group. Black wireframes along each axis illustrate the shape deformations in relation to the mean shape (dashed wireframes) associated with moving from one extreme PC score to another in the medio-lateral (ML) and proximo-distal (PD) profiles of the tibia. The inset (top right) shows the wireframes superimposed on a sample bone viewed in ML and PD profiles. TSV, total shape variance.

Journal of Experimental Biology (2019) 222, jeb203125. doi:10.1242/jeb.203125

Table 2. Least squares means and standard errors of the bending strength at the tibia midshaft in the three lines, estimated at the covariate mean body mass (36.18 g)

Property	LS1 (*n*=23)	LS2 (*n*=25)	Control (*n*=17)
Body mass (g)	38.689 (1.121)^{C}	35.184 (0.604)	34.565 (1.012)
Tibia length (mm)	19.972 (0.108)^{C}	19.96 (0.099)^{C}	17.846 (0.122)^{LS1,LS2}
Yield moment (N mm)	23.064 (1.33)	25.333 (1.206)	22.377 (1.504)
Maximum moment (N mm)	25.26 (1.46)	26.32 (1.36)	23.97 (1.68)
Fracture moment (N mm)	22.22 (1.67)	22.89 (1.52)	22.92 (1.89)
Normalized displacement to yield (mm mm^{-2})	0.087 (0.009)^{C}	0.093 (0.007)^{C}	0.205 (0.01)^{LS1,LS2}
Normalized post-yield displacement (mm mm^{-2})	0.103 (0.016)^{C}	0.116 (0.015)^{C}	0.22 (0.019)^{LS1,LS2}
Rigidity (N mm^{2})	303.5 (18.53)^{C}	307.19 (16.49)^{C}	136.16 (20.95)^{LS1,LS2}
Work to fracture (N)	3.269 (0.41)^{C}	4.011 (0.384)^{C}	7.368 (0.463)^{LS1,LS2}
Yield strength (MPa)	28.42 (1.77)	31.63 (1.68)	29.25 (2.28)
Ultimate strength (MPa)	30.8 (1.79)	32.88 (1.7)	31.12 (2.31)
E (MPa)	498.44 (28.62)^{C}	517.86 (27.1)^{C}	253.63 (36.81)^{LS1,LS2}

Superscripts denote significant differences in LS means (P<0.05) between a given group and: ^{C}Control, ^{LS1}Longshanks 1, ^{LS2}Longshanks 2 (Tukey's HSD).

We found a statistically significant interaction between line and sex for moment variables; however, this interaction was driven primarily by LS1, in which moments were significantly greater in males than in females from all lines. When pooled by sex, there were no significant differences among lines in mean yield, maximum or fracture moments (Table 2, Fig. 2A). In contrast, the normalized yield and post-yield displacements are significantly shorter in both Longshanks lines, leading to a total displacement that was less than half that of controls. The shorter normalized PYD indicates that Longshanks bones are significantly more brittle. Similarly, the Longshanks tibiae were significantly more rigid (Table 2, Fig. 2A). Taken together, the similar bending moments but different mean normalized deflections in control versus Longshanks tibiae contribute to a mean normalized work-to-fracture in both Longshanks lines that is approximately half its value in the control bone.

Bone tissue mechanical properties

The bone tissue strength properties estimated by combining three-point bending and cross-sectional geometry data were consistent with the whole bone bending data (Fig. 2B, Table 2). Specifically, we found no differences among lines in the yield and ultimate strengths of bone tissue; however, the mean estimated elastic modulus, which reflects the resistance to deformation when bone tissue is loaded, was approximately twice as great in Longshanks as in control tibiae.

Bone tissue composition

There was no difference in mean mass among the F16 females used for bone composition analysis (Table 3). Mean water content was ~8% higher in Longshanks bones, while ash content and dry bone density differed from levels in the control by less than 2%. We found no statistically significant differences among the lines in water content, dry density or in the proportion of mineralized tissue (Fig. 3, Table 3).

DISCUSSION

In this study, we tested whether whole bone and tissue-level mechanical properties, as well as bone composition, were altered by changes in length and shape of the tibia in a mouse selectively bred for greater tibia length relative to body mass. Our shape analysis confirms and extends our previous observations in Longshanks line LS1 at generation F10, in that the tibia in both Longshanks lines has become more gracile at generation F15, when compared to the randomly bred control mice (Cosman et al., 2016). Furthermore, the cross-sectional geometry at the midshaft in all three lines was similar, with the exception of the lower relative cortical area in

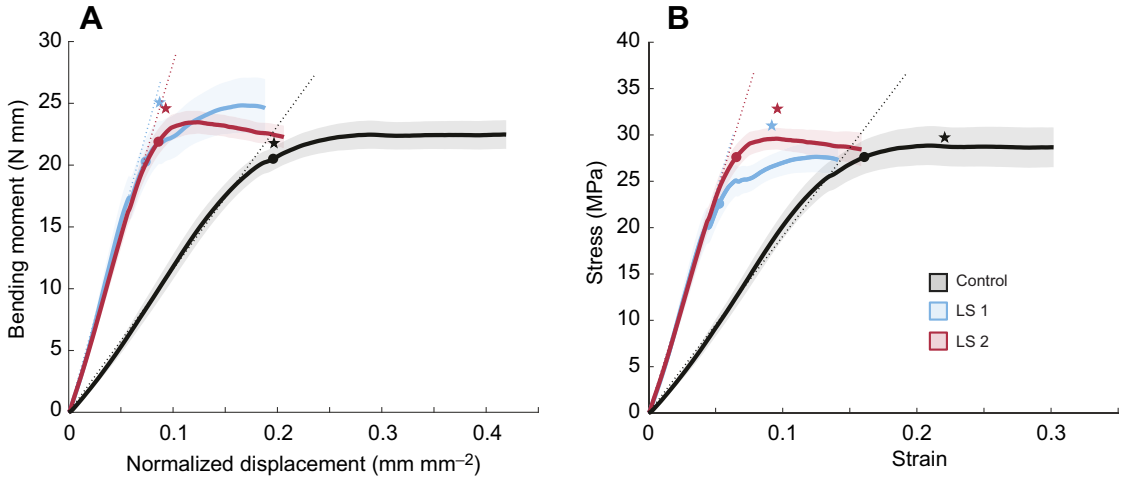

Fig. 2. Mean moment-normalized displacement and stress–strain curves at the tibia midshaft in Longshanks and control mice. (A) Mean moment-normalized displacement curves. (B) Stress–strain curves. Shaded area represents the mean±s.e.m. Dotted lines represent the line of best fit through the linear portion of the mean moment-normalized displacement curves, prior to yield, which is indicated by a dot. The stars denote the normalized yield displacement/strain and yield moments/stress obtained from individual samples, averaged by line (see Table 2). The slopes of the dotted lines represent bending rigidity in A and elastic modulus in B (Table 2).

Journal of Experimental Biology (2019) 222, jeb203125. doi:10.1242/jeb.203125

Table 3. Observed means and standard errors of bone composition and density

Property	LS1 (*n*=8)	LS2 (*n*=8)	Control (*n*=8)
Body mass (g)	32.58 (0.97)	30.57 (0.73)	29.97 (1.32)
Water content (%)	7.98 (0.83)	7.76 (0.88)	7.27 (0.95)
Ash content (%)	62.74 (0.69)	62.98 (0.89)	63.73 (0.47)
Bone density (mg mm^{-3})	1.76 (0.01)	1.74 (0.02)	1.74 (0.02)

Longshanks, which is likely due to their slightly larger endosteal cavities. Our whole bone mechanical testing on the tibia revealed significant differences in the bending behavior of Longshanks versus control bones. In accordance with the broadly similar midshaft cross-sectional properties among lines, we found no differences among lines in the yield, maximum and fracture moments experienced by the tibia in whole bone bending (Fig. 2A). In other words, despite being longer by ∼13% relative to body mass, the Longshanks tibiae remain appropriately buttressed against external bending moments. This pattern holds when looking at tissue-level yield and ultimate strengths, which did not differ significantly among lines (Fig. 2B).

In contrast, Longshanks and control bones exhibited striking differences in their elastic properties. Specifically, in whole bone bending, Longshanks tibiae were significantly more rigid, experiencing bending moments that were over twice as great per unit normalized displacement relative to controls (Fig. 2A, Table 2). Furthermore, normalized displacements to yield and post-yield displacement to fracture were half as great as in controls, indicating that bones were also more brittle, in addition to their increased rigidity. Partly as a result of this increased rigidity and brittleness, the average work required to break a Longshanks tibia was 45–55% lower than that required to break a control tibia. These changes in the elastic properties of the bones were further supported by our observation that a third of control tibiae had to be removed from the strength analysis because their bending displacements exceeded the mechanical tester's maximum travel distance, whereas only ∼14–15% of the Longshanks bones had to be excluded for this reason (3-group chi-square test, χ^2=4.47, P=0.107).

At the tissue level, our estimates of elastic modulus, a measure of the resistance of a unit of bone tissue to deformation when loaded, suggest that the observed increase in rigidity of the Longshanks tibia may arise from changes in the mechanical properties of cortical bone tissue itself, rather than from changes in its cortical geometry or overall shape. Whole bone strength is influenced by both structural and material properties of bones; however, brittleness is thought to reflect the tissue-level material properties of bone, such as bone mineralization and/or bone matrix composition (Jepsen et al., 1996; Jepsen et al., 2001; Wang et al., 2001; Silva et al., 2006). In this context, the greater elastic modulus and brittleness of Longshanks bones suggest that their cortical tissue properties may have been altered as a correlated response to selection for increased relative bone length.

To examine this possibility, we quantified basic bone composition on samples of F16 tibia diaphyses in the three groups. Bone composition data showed that water content, mineral content and dry bone density did not differ among the lines (Fig. 3). These data are in agreement with our previous analyses of the tibia metaphysis and shaft in Longshanks. Using complementary μCT-based methods, Farooq et al. (2017) found that tissue mineral density (TMD) was lower by ∼7% in LS1 compared with controls and LS2, while the TMD of LS2 was the same as in controls. This trend can be observed in the present ash content analysis, although the difference was much smaller, and not statistically significant (∼1.5% lower in LS1 compared with control; Table 3, Fig. 3). We may tentatively exclude mineral content as the basis of brittle bones in Longshanks mice, however, because increased mineralization is associated with increased stiffness/brittleness of bone tissue (Currey, 1999; Jepsen et al., 2001; Mulder et al., 2008). Moreover, Farooq et al. (2017) found no differences in cortical microarchitecture based on high-resolution X-ray microscopy of the tibia diaphysis, including porosity. The lack of changes in tissue mineral composition and microarchitecture suggests that the molecular organization and composition of the organic bony matrix itself may be altered in Longshanks bones in ways that contribute to their brittleness. Future work that directly assesses elastic modulus, cortical matrix composition, including collagen fibril content, orientation and organization (Martin and Ishida, 1989), will help to determine whether selection for longer tibiae altered the molecular and/or developmental properties of brittle bones in Longshanks mice.

Broader implications

We have shown that selection for increased relative tibia length, mediated largely by accelerated longitudinal growth (Marchini and Rolian, 2018), did not alter whole bone bending strength, but substantially increased rigidity and brittleness of the tibia, in as few as 15 generations of selective breeding (∼3.5 years). Although caution is warranted in generalizing from this experimental system, our results have implications for bone mechanical properties in the

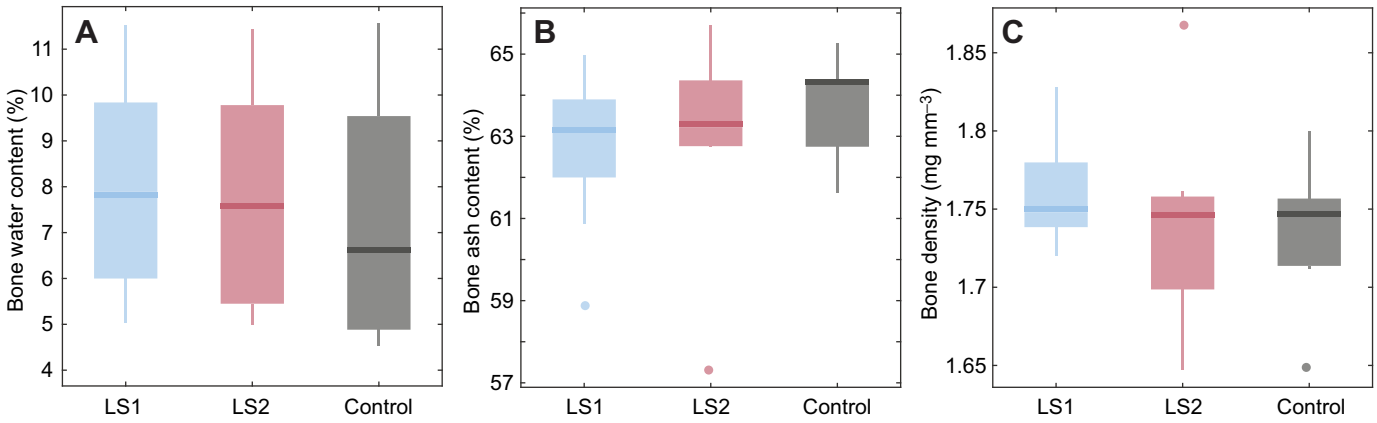

Fig. 3. Tissue composition of the tibia diaphysis. Boxplots show the median (line), interquartile range (box), non-outlier range (whiskers) and outliers (circles) of (A) bone water content, (B) bone ash content and (C) bone density in the two Longshanks lines and in control tibiae.

evolution of functional specializations in other species, both domestic and wild. For example, our data indicate that selection for accelerated skeletal growth can increase bone brittleness. In an analysis comparing domestic white leghorn chickens selectively bred for rapid growth in body mass to their putative ancestral stock, the red junglefowl, Rubin et al. (2007) showed that the former have longer femora, and substantially increased stiffness and reduced PYD, similar to Longshanks mice. This increased brittleness occurred even though the white leghorn's body mass, bone mineral content and cortical geometries also responded to selection in ways that improve bone strength (Rubin et al., 2007; Wright et al., 2010). Similarly, the greyhound, a sprinting dog selectively bred for long, tapered limbs, has significantly stiffer and more brittle bones than the pit bull, which is selectively bred for fighting (Kemp et al., 2004, 2005).

In wild species, evolution of long, tapered limbs related to functional specializations such as sprinting or leaping, could similarly lead to changes in the elastic properties of the long bones, for example, increasing their stiffness while reducing their ductility. Should these long bones experience bending moments that cause deformations beyond the elastic region (i.e. past its yield point), then increased brittleness may make them more prone to fracture. While it is not known how often this happens in the wild, an increased fracture risk presumably carries negative consequences for evolutionary fitness (Bramblett, 1967; Taylor, 1971; Bulstrode et al., 1986; Bertram and Biewener, 1988; Lovell, 1991; Jurmain, 1997; ter Hofstede et al., 2003; Forsman et al., 2006; Carter et al., 2008), and thus over evolutionary timescales, this may favor the correlated evolution of compensatory mechanisms that help to mitigate the impact of long tapered bones on fracture risk. Such mechanisms could include structural changes of the limb long bones, such as fusion of bony elements (Moore et al., 2015) and/or changes in life history traits including delayed skeletal maturation to maintain growth rates within physiologically optimal ranges for bony matrix synthesis. For example, a study of 25 families of non-passerine birds found a positive correlation between wing length and fledgling periods (Carrier and Auriemma, 1992). Powered flight may be ontogenetically delayed in these species in order to maintain limb bone growth rates within a safe range for their structural integrity. Further analyses, especially in mammals, will be necessary to test the complex relationships between life history and skeletal physiology and strength.

Acknowledgements
We thank Jason Anderson and Jessica Theodor for providing access to the SkyScan μCT scanner, Nigel Shrive and Neil Duncan for access to the Bose mechanical tester, and Anne Katzenberg and Kris Markin for facilitating access to the muffle furnace. Many thanks also to Karl Jepsen, John Bertram and Sarah Manske, as well as to the editor and two anonymous reviewers for helpful feedback on previous versions of the manuscript.

Competing interests
The authors declare no competing or financial interests.

Author contributions
Conceptualization: M.C., H.M.B., C.R.; Methodology: M.C., H.M.B., C.R.; Formal analysis: M.C., H.M.B., C.R.; Investigation: M.C., H.M.B., C.R.; Data curation: M.C., C.R.; Writing - original draft: M.C., H.M.B., C.R.; Writing - review & editing: M.C., H.M.B., C.R.; Visualization: C.R.; Supervision: C.R.; Project administration: C.R.; Funding acquisition: C.R.

Funding
This study was supported by Discovery Grant 4181932 from the Natural Sciences and Engineering Research Council of Canada (NSERC) to C.R., by the University of Calgary Faculty of Veterinary Medicine, by an award from the Program for Undergraduate Research Experience (PURE) to M.N.C., and by an NSERC Alexander Graham Bell Canadian Graduate Scholarship and Alberta Innovates Health Services Incentives Scholarship to H.M.B.

Supplementary information
Supplementary information available online at
http://jeb.biologists.org/lookup/doi/10.1242/jeb.203125.supplemental

References
Bertram, J. E. A. and Biewener, A. A. (1988). Bone curvature-sacrificing strength for load predictability. *J. Theor. Biol.* **131**, 75-92. doi:10.1016/S0022-5193(88)80122-X

Biewener, A. A. and Bertram, J. E. (1994). Structural response of growing bone to exercise and disuse. *J. Appl. Physiol.* **76**, 946-955. doi:10.1152/jappl.1994.76.2.946

Bou, J., Casinos, A. and Ocaña, J. (1987). Allometry of the limb long bones of insectivores and rodents. *J. Morphol.* **192**, 113-123. doi:10.1002/jmor.1051920204

Bou, J., Olmos, M. and Casinos, A. (1991). Strengths of the limb bones of birds and small mammals in bending and twisting. *Annales Des Sciences Naturelles-Zoologie Et Biologie Animale* **12**, 197-207.

Bouxsein, M. L. (2005). Determinants of skeletal fragility. *Best Pract. Res. Clin. Rheumatol.* **19**, 897-911. doi:10.1016/j.berh.2005.07.004

Bramblett, C. A. (1967). Pathology in darajani baboon. *Am. J. Phys. Anthropol.* **26**, 331. doi:10.1002/ajpa.1330260308

Bulstrode, C., King, J. and Roper, B. (1986). What happens to wild animals with broken bones. *Lancet* **1**, 29-31. doi:10.1016/S0140-6736(86)91905-7

Carrier, D. R. and Auriemma, J. (1992). A developmental constraint on the fledging time of birds. *Biol. J. Linn. Soc.* **47**, 61-77. doi:10.1111/j.1095-8312.1992.tb00656.x

Carter, M. L., Pontzer, H., Wrangham, R. W. and Peterhans, J. K. (2008). Skeletal pathology in *Pan troglodytes* schweinfurthii in Kibale National Park, Uganda. *Am. J. Phys. Anthropol.* **135**, 389-403. doi:10.1002/ajpa.20758

Christiansen, P. (1999a). Scaling of mammalian long bones: small and large mammals compared. *J. Zool.* **247**, 333-348. doi:10.1111/j.1469-7998.1999.tb00996.x

Christiansen, P. (1999b). Scaling of the limb long bones to body mass in terrestrial mammals. *J. Morphol.* **239**, 167-190. doi:10.1002/(SICI)1097-4687(199902)239:2<167::AID-JMOR5>3.0.CO;2-8

Cosman, M. N., Sparrow, L. M. and Rolian, C. (2016). Changes in shape and cross-sectional geometry in the tibia of mice selectively bred for increases in relative bone length. *J. Anat.* **220**, 940-951. doi:10.1111/joa.12459

Cubo, J. and Casinos, A. (1998). The variation of the cross-sectional shape in the long bones of birds and mammals. *Annales Des Sciences Naturelles-Zoologie Et Biologie Animale* **19**, 51-62. doi:10.1016/S0003-4339(98)80134-2

Currey, J. D. (1999). What determines the bending strength of compact bone? *J. Exp. Biol.* **202**, 2495.

Demes, B., Stern, J. T., Hausman, M. R., Larson, S. G., McLeod, K. J. and Rubin, C. T. (1998). Patterns of strain in the macaque ulna during functional activity. *Am. J. Phys. Anthropol.* **106**, 87-100. doi:10.1002/(SICI)1096-8644(199805)106:1<87::AID-AJPA6>3.0.CO;2-A

Demes, B., Qin, Y.-X., Stern, J. T., Larson, S. G. and Rubin, C. T. (2001). Patterns of strain in the macaque tibia during functional activity. *Am. J. Phys. Anthropol.* **116**, 257-265. doi:10.1002/ajpa.1122

Doube, M., Kłosowski, M. M., Arganda-Carreras, I., Cordelieres, F. P., Dougherty, R. P., Jackson, J. S., Schmid, B., Hutchinson, J. R. and Shefelbine, S. J. (2010). BoneJ Free and extensible bone image analysis in ImageJ. *Bone* **47**, 1076-1079. doi:10.1016/j.bone.2010.08.023

Dryden, I. L. and Mardia, K. V. (1998). *Statistical Shape Analysis*. Chichester, New York: John Wiley & Sons.

Farooq, S., Leussink, S., Sparrow, L. M., Marchini, M., Britz, H. M., Manske, S. L. and Rolian, C. (2017). Cortical and trabecular morphology is altered in the limb bones of mice artificially selected for faster skeletal growth. *Sci. Rep.* **7**, 10527. doi:10.1038/s41598-017-10317-x

Felsenberg, D. and Boonen, S. (2005). The bone quality framework: determinants of bone strength and their interrelationships, and implications for osteoporosis management. *Clin. Ther.* **27**, 1-11. doi:10.1016/j.clinthera.2004.12.020

Fleming, R. H., Whitehead, C. C., Alvey, D., Gregory, N. G. and Wilkins, L. J. (1994). Bone-structure and breaking strength in laying hens housed in different husbandry systems. *Br. Poult. Sci.* **35**, 651-662. doi:10.1080/00071669408417731

Forsman, E. D., Otto, I. A. and Muths, E. (2006). Healed fractures and other abnormalities in bones of small mammals. *Northwest Nat.* **87**, 143-146. doi:10.1898/1051-1733(2006)87[143:HFAOAI]2.0.CO;2

Gregory, N. G. and Wilkins, L. J. (1989). Broken bones in domestic-fowl-handling and processing damage in end-of-lay battery hens. *Br. Poult. Sci.* **30**, 555-562. doi:10.1080/00071668908417179

Heinrich, R. E., Ruff, C. B. and Adamczewski, J. Z. (1999). Ontogenetic changes in mineralization and bone geometry in the femur of muskoxen (Ovibos moschatus). *J. Zool.* **247**, 215-223. doi:10.1111/j.1469-7998.1999.tb00985.x

Hernandez, C. J. and Keaveny, T. M. (2006). A biomechanical perspective on bone quality. *Bone* **39**, 1173-1181. doi:10.1016/j.bone.2006.06.001

Jepsen, K. J., Goldstein, S. A., Kuhn, J. L., Schaffler, M. B. and Bonadio, J. (1996). Type-I collagen mutation compromises the post-yield behavior of Mov13 long bone. *J. Orthop. Res.* **14**, 493-499. doi:10.1002/jor.1100140320

Jepsen, K. J., Pennington, D. E., Lee, Y. L., Warman, M. and Nadeau, J. (2001). Bone brittleness varies with genetic background in A/J and C57BL/6J inbred mice. *J. Bone Miner. Res.* **16**, 1854-1862. doi:10.1359/jbmr.2001.16.10.1854

Jepsen, K. J., Akkus, O., Majeska, R. J. and Nadeau, J. H. (2003). Hierarchical relationship between bone traits and mechanical properties in inbred mice. *Mamm. Genome* **14**, 97-104. doi:10.1007/s00335-002-3045-y

Jepsen, K. J., Silva, M. J., Vashishth, D., Guo, X. E. and van der Meulen, M. C. H. (2015). Establishing biomechanical mechanisms in mouse models: practical guidelines for systematically evaluating phenotypic changes in the diaphyses of long bones. *J. Bone Miner. Res.* **30**, 951-966. doi:10.1002/jbmr.2539

Jurmain, R. (1997). Skeletal evidence of trauma in African apes, with special reference to the Gombe chimpanzees. *Primates* **38**, 1-14. doi:10.1007/BF02385918

Kemp, T. J., Bachus, K. N., Nairn, J. A. and Carrier, D. R. (2004). Mechanical properties of limb bones in dogs specialized for running versus fighting. *Integr. Comp. Biol.* **44**, 712-712.

Kemp, T. J., Bachus, K. N., Nairn, J. A. and Carrier, D. R. (2005). Functional trade-offs in the limb bones of dogs selected for running versus fighting. *J. Exp. Biol.* **208**, 3475-3482. doi:10.1242/jeb.01814

Klingenberg, C. P. (2011). MorphoJ: an integrated software package for geometric morphometrics. *Mol. Ecol. Resour.* **11**, 353-357. doi:10.1111/j.1755-0998.2010.02924.x

Lieberman, D. E., Pearson, O. M., Polk, J. D., Demes, B. and Crompton, A. W. (2003). Optimization of bone growth and remodeling in response to loading in tapered mammalian limbs. *J. Exp. Biol.* **206**, 3125-3138. doi:10.1242/jeb.00514

Lieberman, D. E., Polk, J. D. and Demes, B. (2004). Predicting long bone loading from cross-sectional geometry. *Am. J. Phys. Anthropol.* **123**, 156-171. doi:10.1002/ajpa.10316

Lovell, N. C. (1991). An evolutionary framework for assessing illness and injury in nonhuman-primates. *Yearb. Phys. Anthropol.* **34**, 117-155. doi:10.1002/ajpa.1330340608

Main, R. P. and Biewener, A. A. (2007). Skeletal strain patterns and growth in the emu hindlimb during ontogeny. *J. Exp. Biol.* **210**, 2676-2690. doi:10.1242/jeb.004580

Marchini, M. and Rolian, C. (2018). Artificial selection sheds light on developmental mechanisms of limb elongation. *Evolution* **72**, 825-837. doi:10.1111/evo.13447

Marchini, M., Sparrow, L. M., Cosman, M. N., Dowhanik, A. S., Krueger, C. B., Hallgrimsson, B. and Rolian, C. (2014). Impacts of genetic correlation on the independent evolution of body mass and skeletal size in mammals. *BMC Evol. Biol.* **14**, 258. doi:10.1186/s12862-014-0258-0

Martin, R. B. and Ishida, J. (1989). The relative effects of collagen fiber orientation, porosity, density, and mineralization on bone strength. *J. Biomech.* **22**, 419. doi:10.1016/0021-9290(89)90202-9

Moore, T. Y., Organ, C. L., Edwards, S. V., Biewener, A. A., Tabin, C. J., Jenkins, F. A., , Jr and Cooper, K. L. (2015). Multiple phylogenetically distinct events shaped the evolution of limb skeletal morphologies associated with bipedalism in the jerboas. *Curr. Biol.* **25**, 2785-2794. doi:10.1016/j.cub.2015.09.037

Mulder, L., Koolstra, J. H., den Toonder, J. M. J. and van Eijden, T. M. G. J. (2008). Relationship between tissue stiffness and degree of mineralization of developing trabecular bone. *J. Biomed. Mater. Res. A* **84A**, 508-515. doi:10.1002/jbm.a.31474

O'Neill, M. C. and Ruff, C. B. (2004). Estimating human long bone cross-sectional geometric properties: a comparison of noninvasive methods. *J. Hum. Evol.* **47**, 221-235. doi:10.1016/j.jhevol.2004.07.002

Polk, J. D., Demes, B., Jungers, W. L., Biknevicius, A. R., Heinrich, R. E. and Runestad, J. A. (2000). A comparison of primate, carnivoran and rodent limb bone cross-sectional properties: are primates really unique? *J. Hum. Evol.* **39**, 297-325. doi:10.1006/jhev.2000.0420

Pontzer, H., Lieberman, D. E., Momin, E., Devlin, M. J., Polk, J. D., Hallgrimsson, B. and Cooper, D. M. L. (2006). Trabecular bone in the bird knee responds with high sensitivity to changes in load orientation. *J. Exp. Biol.* **209**, 57-65. doi:10.1242/jeb.01971

Ramzan, P. H. L. and Palmer, L. (2011). Musculoskeletal injuries in Thoroughbred racehorses: a study of three large training yards in Newmarket, UK (2005-2007). *Vet. J.* **187**, 325-329. doi:10.1016/j.tvjl.2009.12.019

Rasband, W. (2014). *ImageJ. U. S. National Institutes of Health*. Bethesda, MD.

Rubin, C. T. (1984). Skeletal strain and the functional-significance of bone architecture. *Calcif. Tissue Int.* **36**, S11-S18. doi:10.1007/BF02406128

Rubin, C. J., Brandstrom, H., Wright, D., Kerje, S., Gunnarsson, U., Schutz, K., Fredriksson, R., Jensen, P., Andersson, L., Ohlsson, C. et al. (2007). Quantitative trait loci for BMD and bone strength in an intercross between domestic and wildtype chickens. *J. Bone Miner. Res.* **22**, 375-384. doi:10.1359/jbmr.061203

Ruff, C. B. (2000). Body size, body shape, and long bone strength in modern humans. *J. Hum. Evol.* **38**, 269-290. doi:10.1006/jhev.1999.0322

Ruff, C. (2003). Ontogenetic adaptation to bipedalism: age changes in femoral to humeral length and strength proportions in humans, with a comparison to baboons. *J. Hum. Evol.* **45**, 317-349. doi:10.1016/j.jhevol.2003.08.006

Ruff, C. B., Burgess, M. L., Bromage, T. G., Mudakikwa, A. and McFarlin, S. C. (2013). Ontogenetic changes in limb bone structural proportions in mountain gorillas (*Gorilla beringei berirtgei*). *J. Hum. Evol.* **65**, 693-703. doi:10.1016/j.jhevol.2013.06.008

Sarringhaus, L. A., MacLatchy, L. M. and Mitani, J. C. (2016). Long bone cross-sectional properties reflect changes in locomotor behavior in developing chimpanzees. *Am. J. Phys. Anthropol.* **160**, 16-29. doi:10.1002/ajpa.22930

Silva, M. J., Brodt, M. D., Wopenka, B., Thomopoulos, S., Williams, D., Wassen, M. H. M., Ko, M., Kusano, N. and Bank, R. A. (2006). Decreased collagen organization and content are associated with reduced strength of demineralized and intact bone in the SAMP6 mouse. *J. Bone Miner. Res.* **21**, 78-88. doi:10.1359/JBMR.050909

Slice, D. E. (2005). *Modern Morphometrics in Physical Anthropology*. New York: Kluwer Academic/Plenum Publishers.

Taylor, M. E. (1971). Bone diseases and fractures in east African viverridae. *Can. J. Zool.* **49**, 1035. doi:10.1139/z71-159

ter Hofstede, H. M., Miller, J., Ratcliffe, J. M. and Fenton, M. B. (2003). A healed fractured radius in a flying big brown bat (*Eptesicus fuscus*). *J. Wildlife Rehabil* **26**, 4-7.

Turner, C. H. and Burr, D. B. (1993). Basic biomechanical measurements of bone - a tutorial. *Bone* **14**, 595-608. doi:10.1016/8756-3282(93)90081-k

van Lenthe, G. H., Voide, R., Boyd, S. K. and Muller, R. (2008). Tissue modulus calculated from beam theory is biased by bone size and geometry: Implications for the use of three-point bending tests to determine bone tissue modulus. *Bone* **43**, 717-723. doi:10.1016/j.bone.2008.06.008

Wallace, I. J., Demes, B., Mongle, C., Pearson, O. M., Polk, J. D. and Lieberman, D. E. (2014). Exercise-induced bone formation is poorly linked to local strain magnitude in the sheep tibia. *PLoS ONE* **9**, e99108. doi:10.1371/journal.pone.0099108

Wang, X. D., Bank, R. A., TeKoppele, J. M. and Agrawal, C. M. (2001). The role of collagen in determining bone mechanical properties. *J. Orthop. Res.* **19**, 1021-1026. doi:10.1016/S0736-0266(01)00047-X

Wright, D., Rubin, C.-J., Barrio, A. M., Schütz, K., Kerje, S., Brändström, H., Kindmark, A., Jensen, P. and Andersson, L. (2010). The genetic architecture of domestication in the chicken: effects of pleiotropy and linkage. *Mol. Ecol.* **19**, 5140-5156. doi:10.1111/j.1365-294X.2010.04882.x

Young, J. W., Fernandez, D. and Fleagle, J. G. (2010). Ontogeny of long bone geometry in capuchin monkeys (*Cebus albifrons* and *Cebus apella*): implications for locomotor development and life history. *Biol. Lett.* **6**, 197-200. doi:10.1098/rsbl.2009.0773

Young, J. W., Danczak, R., Russo, G. A. and Fellmann, C. D. (2014). Limb bone morphology, bone strength, and cursoriality in lagomorphs. *J. Anat.* **225**, 403-418. doi:10.1111/joa.12220

Dataset 1. Raw data for all shape, cross-sectional, strength and ash analyses.

Click here to Download Dataset 1